

Monte Carlo Studies of Adsorbed Monolayers: Lattice–Gas Models with Translational Degrees of Freedom

M. Presber

*Institut für Physik, Johannes Gutenberg–Universität Mainz,
Staudingerweg 7, Postfach 3980, D–55099 Mainz, Germany*

B. Dünweg

*Max–Planck–Institut für Polymerforschung,
Ackermannweg 10, D–55128 Mainz, Germany*

D. P. Landau

*Center for Simulational Physics, The University of Georgia,
Athens, GA 30602, USA*

(February 9, 1998)

Abstract

Standard lattice–gas models for the description of the phase behavior of adsorbed monolayers are generalized to “elastic lattice gases” which allow for translational degrees of freedom of the adsorbate atoms but have the substrate lattice structure built into the adsorbate–adsorbate interaction. For such models, we derive a simple and efficient grand–canonical Monte Carlo algorithm, which treats the occupied and empty sites in precisely the same way. Using this method, we calculate the phase diagram of a simple model for the adsorption of hydrogen on palladium (100); this model includes only pairwise interactions and exhibits an ordered $c(2 \times 2)$ structure. For our choice of parameters, we find only a rather small influence of the translational degrees of freedom on the phase diagram. In particular, the observed asymmetry, albeit clearly present, is quite weak. Finite–size scaling reveals that the second–order phase transition between $c(2 \times 2)$ and the disordered phase is Ising–like, i. e. the elastic degrees of freedom do not change the universality class.

05.50.+q, 05.70.Jk, 64.60.Cn, 64.60.Kw, 68.35.Rh

I. INTRODUCTION

The phase behavior of adsorbed monolayers on a substrate has found longstanding interest [1], both experimental [2–4] as well as theoretical [5–14]. Usually the theoretical description is done in the framework of lattice–gas models, where the substrate is a fixed lattice with fixed adsorption sites which can either be occupied or empty. Such a model is equivalent to an Ising model, where an occupied site corresponds to an “up” pseudospin, while empty sites are modeled as “down” pseudospins. The rich phase behavior (gas–liquid transition as well as the formation of various superstructures with second–order phase transitions belonging to a variety of two–dimensional universality classes [5,6]) is then investigated using interaction parameters like nearest neighbor, next–nearest neighbor, . . . , attraction or repulsion. However, it is well–known, and obvious from the transformation to the Ising model (see also Sec. II), that pair interactions will always produce a phase diagram in the temperature–coverage (T – Θ) plane which is symmetric around $\Theta = 1/2$. This is a direct consequence of the inherent particle–hole symmetry of the model. The most common approach to breaking this symmetry is the introduction of three–body interactions [11–13]. Without these terms, it is in many cases impossible to obtain a reasonable fit to experimental phase diagrams, which quite often exhibit a marked asymmetry.

On the other hand, the gas–liquid transition phase diagram in a simple fluid usually exhibits a substantial asymmetry, too. This is however not due to three–body interactions between the particles, but rather to the simple fact that they can freely move in space, such that there is no notion of free sites, and consequently no particle–hole symmetry. Based on this observation, one should expect that one can also break the symmetry by allowing for additional translational degrees of freedom of the adsorbate atoms, while still strictly sticking to two–body interactions. Persson [15] has argued quite convincingly along these lines.

Of course, such a system can be studied by straightforward Molecular Dynamics (MD) simulation [16] of a number of particles subject to an external potential which models the effect of the substrate. Similarly, the system could also be studied by using a standard Monte Carlo (MC) algorithm in the canonical ensemble [17]. However, these approaches have a number of disadvantages when it comes to the accurate quantitative analysis of phase transitions and critical phenomena. The conserved particle number will, in case of a first–order phase transition, generate two coexisting phases separated by an interface. This requires, on the one hand, sufficiently large systems such that the structure of the interface, and the competition of the interfacial free energy with the bulk free energy, is simulated correctly. On the other hand, long runs are also required in order to equilibrate the interfacial structure — the conservation law induces a slow decay of density fluctuations (“hydrodynamic slowing down”) [18]. Therefore, one would prefer a simulation method which suppresses the occurrence of the interface, i. e. a grand–canonical algorithm [19–23] (note that both constant–pressure schemes [24] as well as the Gibbs ensemble method [25] are not feasible due to the rigid structure of the substrate).

While it has been demonstrated that grand–canonical simulations of atomic models are able to study phase equilibria and critical phenomena with high accuracy [22,23], such a method (or model) is nevertheless computationally rather demanding, at least when compared to simulations of simple lattice–gas/Ising models. We therefore seek a simplified model, which still includes the translational degrees of freedom, and works in the grand–canonical ensemble, but nevertheless resembles more closely a simple lattice–gas model, thus retaining some aspects which allow “cheaper” simulations. The main simplifications of our

model are (i) reduction of the translational degrees of freedom to two dimensions, and (ii) keeping the lattice–gas notion of an adsorption site which can be either occupied or empty, such that the simulation allows only for a maximum number of adsorbed atoms. Although the (occupied or empty) sites can move in space, the neighbor relations between the sites are kept fixed, such that the same neighbor table can be used throughout a run. Moreover, occupied and empty sites are treated in precisely the same fashion, such that the Monte Carlo updates are just site moves and pseudospin flips. The resulting algorithm is quite simple, compact, and efficient, permitting full vectorization based on the standard checkerboard method. Such an approach is quite analogous to semi–grand canonical simulations of binary alloys on a distortable lattice [26,27]; however, the decisive difference is that we now assign an *artificial* translational degree of freedom to a “ghost particle” (empty site) which, in reality, simply does not exist. This requires some care in the construction and optimization of the MC algorithm, which is done in a similar spirit as in previous “ghost particle” method simulations of adsorbates [20,21], which however did not impose any fixed neighbor structure. This fixed lattice structure is also the main difference to a recent study of two–dimensional phase transitions of systems with coupled internal and translational degrees of freedom [28], which however used a random lattice with fluctuating neighbor shells. It should be mentioned that an additional advantage of such a pre–defined lattice structure is a simplification of the data analysis; the definition of sublattices and order parameters etc. remains trivial.

The remainder of this paper is organized as follows: Sec. II contains most of the theoretical development. Starting from a physical Hamiltonian, we perform the transformation to the grand–canonical ensemble, and derive the Monte Carlo algorithm. The effective Hamiltonian, which governs the simulation procedure, no longer exhibits any particle–hole symmetry. Moreover, the Ising model notion of a magnetic field (which, in the simple lattice–gas case, would describe the symmetry of the phase diagram in the grand–canonical ensemble), no longer makes sense, due to an arbitrary choice of the zero of the chemical potential (see Sec. II). Sec. III then describes how the algorithm is applied to a specific model on the square lattice with nearest and next–nearest neighbor interactions; the results for the phase diagram and the critical behavior are presented in Sec. IV. The model is a straightforward generalization of a simple lattice gas which has been studied by one of the present authors long ago [9] in order to describe the behavior of H/Pd (100), which forms an ordered $c(2 \times 2)$ phase around $\Theta = 1/2$. In the limit of vanishing elastic interactions, our model reduces to the case of Ref. [9]. Finally, Sec. V concludes with a brief summary.

II. GRAND–CANONICAL SIMULATIONS OF ELASTIC LATTICE GASES

Our starting point is a distortable lattice of N sites in d –dimensional space. These sites are allowed to move freely in a simulation box, with periodic boundary conditions, whose size defines the system volume V . The position of the i th site is denoted by \vec{r}_i . To determine the distances between sites we impose the standard minimum image convention [29]. If the lattice is perfectly ordered, the movable sites are located at their ideal positions, $\vec{r}_i = \vec{r}_i^0$; these are the ideal adsorption sites. From the topology of that ordered lattice (e. g. square lattice) one derives the neighborhood relations between the sites (nearest neighbors $\langle ij \rangle$, next–nearest neighbors $\langle\langle ij \rangle\rangle$, etc.), which are viewed as a property of the lattice as such, independently of any interactions, and independently of the configuration in position space.

Now M sites out of the N possible ones are selected and occupied with particles. We

denote these sites with i_1, i_2, \dots, i_M , while the empty sites are $i_{M+1}, i_{M+2}, \dots, i_N$. By requiring both $i_1 < i_2 < \dots < i_M$ and $i_{M+1} < i_{M+2} < \dots < i_N$, each occupation configuration corresponds uniquely to one index assignment. Alternatively, an occupation configuration is described by the standard lattice gas variables c_i , where $c_{i_1} = c_{i_2} = \dots = c_{i_M} = 1$ and $c_{i_{M+1}} = c_{i_{M+2}} = \dots = c_{i_N} = 0$, or the pseudospin variables $S_i = 2c_i - 1 = \pm 1$.

An interaction between particles can only occur if they are nearest or next-nearest neighbors on the lattice. If two particles are rather close to each other in real space, but third-nearest (or further) neighbors with respect to the imposed lattice topology, they will not interact. The restriction to nearest and next-nearest neighbors is only done for simplicity of notation; inclusion of additional neighbor shells, triplet interactions etc. is trivial. The decisive simplification is that the interaction cutoff is not determined via the configuration in real space, but rather via the lattice. We now introduce a characteristic function for nearest neighbors,

$$\omega_{nn}(i, j) = \begin{cases} 1 & (i, j) \text{ nearest neighbors} \\ 0 & \text{otherwise,} \end{cases} \quad (2.1)$$

and similarly ω_{nnn} for next-nearest neighbors. Then the Hamiltonian can be written as

$$\begin{aligned} \mathcal{H} = & \sum_{k=1}^M v_0 (\vec{r}_{i_k} - \vec{r}_{i_k}^0) \\ & + \sum_{k=1}^{M-1} \sum_{l=k+1}^M \omega_{nn}(i_k, i_l) v_{nn} (\vec{r}_{i_k} - \vec{r}_{i_l}) \\ & + \sum_{k=1}^{M-1} \sum_{l=k+1}^M \omega_{nnn}(i_k, i_l) v_{nnn} (\vec{r}_{i_k} - \vec{r}_{i_l}), \end{aligned} \quad (2.2)$$

using nearest and next-nearest neighbor potentials v_{nn} and v_{nnn} as well as a substrate potential v_0 , which binds each particle to its ideal site. The canonical partition function of that M -particle system is then

$$Z_{can}(M) = \sum_{\{c_i\}_M} V_0^{-M} \int d\vec{r}_{i_1} \int d\vec{r}_{i_2} \dots \int d\vec{r}_{i_M} \exp(-\beta \mathcal{H}(\{\vec{r}_{i_k}\})). \quad (2.3)$$

Here, we sum over all possibilities to distribute M particles onto the N -site lattice. V_0 is an arbitrary normalization volume which is necessary to render the partition function dimensionless. Within the quasi-classical approximation, V_0 is usually associated with the thermal de Broglie wave length; however, within the framework of strictly classical statistical physics it is just a normalization constant whose value does not matter for the physics. Usually we will choose $V_0 = a^d$, where a is the lattice constant of the perfect lattice. The integrations extend over the volume of the simulation box; note that only the coordinates of the occupied sites are integrated over — only these are the physical degrees of freedom. As usual, $\beta = (k_B T)^{-1}$. The grand-canonical partition function then is

$$Z_{gc} = \sum_{M=0}^N \exp(\beta \mu M) Z_{can}(M), \quad (2.4)$$

where μ denotes the chemical potential. It should be noted that the lattice induces a unique labeling of the particles (which has explicitly been given above), such that they must be viewed as *distinguishable*. For this reason, a permutation factor $(M!)^{-1}$ does *not* appear.

Now let us assume that a Monte Carlo simulation is run, where a simple Metropolis algorithm is applied to the effective Hamiltonian

$$\begin{aligned}
\mathcal{H}_{eff} = & \sum_{i=1}^N c_i \left(v_0 \left(\vec{r}_i - \vec{r}_i^0 \right) - \mu - \alpha k_B T \right) \\
& + \sum_{i=1}^N (1 - c_i) U_0 \left(\vec{r}_i - \vec{r}_i^0 \right) \\
& + \sum_{\langle ij \rangle} c_i c_j v_{nn} \left(\vec{r}_i - \vec{r}_j \right) \\
& + \sum_{\langle\langle ij \rangle\rangle} c_i c_j v_{nnn} \left(\vec{r}_i - \vec{r}_j \right),
\end{aligned} \tag{2.5}$$

where c_i and \vec{r}_i are treated as completely independent degrees of freedom of an N -particle system. The parameter α and the potential U_0 will be specified below.

This algorithm will be correct, i. e. produce configurations satisfying the correct probability distribution, if the corresponding partition function

$$Z_{eff} = V_0^{-N} \sum_{\{c_i\}} \int d\vec{r}_1 \dots \int d\vec{r}_N \exp(-\beta \mathcal{H}_{eff}) \tag{2.6}$$

is (up to a constant prefactor) identical to the grand-canonical partition function Z_{gc} according to Eqn. 2.4. The physical motivation for Eqn. 2.5 is as follows: The factors c_i make sure that potential contributions occur only from real particles. Hence, the potential part of \mathcal{H}_{eff} is identical to \mathcal{H} . The term proportional to μ describes the effect of the external chemical potential. The remaining two terms are counter-terms against the intrinsic tendency to “evaporate” at higher temperatures: Without the confining potential U_0 , which binds the “ghosts” close to the ideal adsorption sites, they would move around freely. Therefore, the “ghost” state would be strongly entropically favored, by a translational entropy of $\ln(V/V_0)$ per “ghost” particle. Even worse, this entropic driving force would diverge in the thermodynamic limit. While this pathology could be remedied by the term $\alpha k_B T$ alone, using a proper, system-size dependent choice of α , U_0 is also very important for *dynamical* reasons: We wish to model the potentials v_{nn} , v_{nnn} , v_0 via springs with infinite range of interaction. Suppose a site has escaped its proper local environment in the “ghost” state. It will then be very hard for this site to be turned back into the “real particle” state, because this change would introduce extremely strongly stretched springs into the system, i. e. a very high excitation energy. Therefore the site will diffuse freely in the “ghost” state, until it happens to come back close enough to its proper environment, such that it can re-materialize again. We therefore expect, from random-walk arguments, that the algorithm without the confining potential U_0 would exhibit a correlation time $\tau \propto L^2$, where L is the system linear dimension. In other words, the method would be hampered by an artificial “critical slowing down” everywhere in the phase diagram! We therefore view the introduction of U_0 as an indispensable feature of the method.

In order to find the proper choices for U_0 and α , we have to compare Z_{eff} with Z_{gc} . To this end, we first introduce the partition function of a single particle in the potential U_0 ,

$$\zeta = V_0^{-1} \int d\vec{r} \exp(-\beta U_0(\vec{r})). \tag{2.7}$$

Using the trivial identities $\sum_{\{c_i\}} = \sum_M \sum_{\{c_i\}|_M}$, $\sum_i c_i = M$ and $\sum_i (1 - c_i) = N - M$, we can integrate out the “ghost” degrees of freedom to obtain

$$Z_{eff} = \sum_{M=0}^N \exp(\beta\mu M) \exp(\alpha M) \zeta^{N-M} Z_{can}(M). \quad (2.8)$$

In order to weight every term $Z_{can}(M)$ correctly, we have to choose

$$\alpha = \ln \zeta, \quad (2.9)$$

resulting in

$$Z_{eff} = \zeta^N Z_{gc}. \quad (2.10)$$

The systems are thermodynamically equivalent if the prefactor ζ^N can be viewed as a constant. In order to avoid temperature dependence of ζ , we choose a square-well potential

$$U_0(r) = \begin{cases} 0 & r < R \\ \infty & r > R, \end{cases} \quad (2.11)$$

where the cutoff radius R is of the same order of magnitude as the typical particle displacement from the ideal site. For $|\vec{r}_i - \vec{r}_i^0| > R$, de-materialization is forbidden. Therefore, in two dimensions we have

$$\zeta = \frac{\pi R^2}{V_0}, \quad (2.12)$$

$$\alpha = \ln \left(\frac{\pi R^2}{V_0} \right). \quad (2.13)$$

These choices ensure a correct simulation of the grand-canonical ensemble. In practice, one has to use an effective chemical potential

$$\mu_{eff} = \mu + k_B T \ln \zeta. \quad (2.14)$$

Note that the arbitrary normalization volume V_0 , although explicitly appearing in the above formulae, does *not* enter the effective Hamiltonian \mathcal{H}_{eff} , as it should be — the physical properties of the system should not depend on V_0 . The reason for this independence is simply the fact that the chemical potential μ can only be defined *after* V_0 has been specified, such that μ depends on V_0 , too. Indeed, from statistical thermodynamics it follows that

$$\begin{aligned} \mu &= -k_B T \frac{\partial}{\partial M} \ln Z_{can}(M) \\ &= k_B T \ln V_0 + \frac{\partial}{\partial M} \sum_{\{c_i\}_M} \int d\vec{r}_{i_1} \int d\vec{r}_{i_2} \dots \int d\vec{r}_{i_M} \exp(-\beta \mathcal{H}(\{\vec{r}_{i_k}\})), \end{aligned} \quad (2.15)$$

such that the dependence on V_0 in μ_{eff} exactly cancels out. From these considerations, one sees that a particularly convenient normalization of the partition functions and the chemical potential is given by the choice $V_0 = \pi R^2$, i. e. the normalization volume equals the cutoff volume of the algorithm. In this case, $\zeta = 1$, and $\mu_{eff} = \mu$. In the present study, this has however not been done; we rather chose $V_0 = a^2$ and $R = a$, where a is the lattice constant of the undistorted lattice.

In order to make the asymmetry induced by the translational degrees of freedom more transparent, we transform \mathcal{H}_{eff} to pseudospin variables via $c_i = (S_i + 1)/2$. Without writing down the resulting formulae in full detail, we would just like to point out that the Hamiltonian assumes the form

$$\mathcal{H}_{eff} = \mathcal{H}_0(\{\vec{r}_i\}) - \sum_{\langle ij \rangle} J_{ij}(\{\vec{r}_i\}) S_i S_j - \sum_{\langle\langle ij \rangle\rangle} J_{ij}(\{\vec{r}_i\}) S_i S_j - \sum_i H_i(\{\vec{r}_i\}) S_i. \quad (2.16)$$

The decisive point is that each pseudospin is subject to its own local magnetic field, which depends on the configuration of the sites in space. In the simple lattice gas, the field is a *global* quantity, $H_i \equiv H$, such that the transformation $S_i \rightarrow -S_i$ accompanied with $H \rightarrow -H$ leaves the Hamiltonian invariant. Such a transformation is impossible in the present case, and hence the particle–hole symmetry is no longer present.

III. MODEL, AND MONTE CARLO SIMULATION METHOD

We have studied $L \times L$ square lattices, with $L = 10, 20, 30, 100$, whose lattice constant (in the ideally ordered state $\{\vec{r}_i^0\}$) is denoted by a . Every length is measured in units of a . Similarly, we choose an energy scale $J > 0$ and measure energies in units of J and temperatures in units of J/k_B . The Hamiltonian of Eqn. 2.2 is then specified via

$$\begin{aligned} v_0(r) &= \frac{k_0}{2} r^2 \\ v_{nn}(r) &= \varphi_{nn} + \frac{k_{nn}}{2} (r - l_{nn})^2 \\ v_{nnn}(r) &= \varphi_{nnn} + \frac{k_{nnn}}{2} (r - l_{nnn})^2. \end{aligned} \quad (3.1)$$

For simplicity, we chose the following parameters: $\varphi_{nn} = +4$, $\varphi_{nnn} = -4$, $k_0 = k_{nn} = k_{nnn} = 1$, $l_{nn} = 1$, $l_{nnn} = \sqrt{2}$. The choice of l_{nn} and l_{nnn} ensures that for $\vec{r}_i = \vec{r}_i^0$ the elastic contributions to the Hamiltonian vanish. Since these terms are also positive, one sees that the ground state is obtained for the perfectly ordered lattice $\vec{r}_i = \vec{r}_i^0$. Of course, this is just the simplest case; for choices of l_{nn} and l_{nnn} which introduce a mismatch between the substrate and the adsorbate system one should expect substantially more complicated behavior. The harmonic potentials were chosen as rather soft. This is probably somewhat unrealistic in comparison with experimental systems, but was introduced for reasons of simplicity, and also because we expected the strongest influence of the translational degrees of freedom for a rather soft lattice. The constant offset in v_0 was set to zero, because it can be absorbed in the definition of the chemical potential μ . Finally, for φ_{nn} and φ_{nnn} we note that for $\vec{r}_i = \vec{r}_i^0$ the model reduces to an Ising model with nearest and next–nearest neighbor couplings, $J_{nn} = -1$ (antiferromagnetic) and $J_{nnn} = +1$ (ferromagnetic), respectively.

This latter model (with exactly this set of nn– and nnn–coupling) has already been studied in quite some detail in Ref. [9], whose data serve as a valuable reference state for the present study. The ground state in the grand–canonical ensemble is simply given by a completely filled lattice $(1 \times 1)_+$ for $\mu > 8$, a completely empty lattice $(1 \times 1)_-$ for $\mu < -8$, and an ordered $c(2 \times 2)$ structure for $-8 < \mu < 8$. This latter structure corresponds to a decomposition into two sublattices a and b , each connected via next–nearest neighbor bonds, of whom one is occupied and the other one empty ($\Theta = 1/2$). A physical realization of this structure is the superstructure of hydrogen on a palladium (100) surface.

We therefore sampled moments of the distribution of the order parameter corresponding to the $c(2 \times 2)$ structure, i. e. the staggered magnetization

$$m_{st} = N^{-1} \left(\sum_{i \in a} S_i - \sum_{i \in b} S_i \right). \quad (3.2)$$

It should be noted that the distribution of m_{st} is strictly symmetric around zero. This symmetry is not related to any particle–hole symmetry (which is of course lacking in our model), but rather to the strict equivalence of the two sublattices a and b , which is a purely geometric property. Hence we studied $\langle |m_{st}| \rangle$, the staggered susceptibility

$$\chi_{st} = \frac{N}{T} \left(\langle m_{st}^2 \rangle - \langle |m_{st}| \rangle^2 \right), \quad (3.3)$$

and the fourth–order cumulant [30]

$$U_L = 1 - \frac{\langle m_{st}^4 \rangle}{3 \langle m_{st}^2 \rangle^2}. \quad (3.4)$$

Further quantities of interest are the coverage

$$\Theta = N^{-1} \sum_i \langle c_i \rangle \quad (3.5)$$

and the moment ratio

$$W_L = \frac{\langle m_{st}^2 \rangle}{\langle |m_{st}| \rangle^2}. \quad (3.6)$$

The chemical potential normalization at nonzero temperature was fixed by setting $V_0 = 1$. Furthermore, the cutoff radius R for the confining potential U_0 (cf. Eqn. 2.11) was also chosen as $R = 1$. Tests showed that this is a reasonable choice for ensuring sufficiently fast equilibration, while very large or very small values will both substantially slow the simulation down. We used “compound moves”, where for a single site we generated a new trial configuration for *all* degrees of freedom simultaneously, i. e.

$$\begin{aligned} x'_i &= x_i + f(u_1 - 1/2) \\ y'_i &= y_i + f(u_2 - 1/2) \\ c'_i &= [2u_3], \end{aligned} \quad (3.7)$$

where u_k stands for a random number uniformly distributed in the unit interval $0 < u_k < 1$, and $[...]$ denotes the integer part. This trial move was then accepted or rejected via the standard Metropolis criterion, using \mathcal{H}_{eff} . We chose $f = 0.8$, ensuring an acceptance rate of roughly 1/2 in the relevant temperature regime. The algorithm was fully vectorized based on a four–sublattice checkerboard method and attained 0.48×10^6 particle updates per second on a single Cray Y–MP processor. Typical production runs near second–order phase transitions used between 5×10^5 and 1×10^6 Monte Carlo steps (MCS, sweeps through the lattice).

IV. RESULTS

A. Phase Diagram

The phase diagram in the grand–canonical ensemble, i. e. the (μ, T) –plane, is shown in Fig. 1. At high temperatures, the transition line between the ordered and the disordered phase is of second order, while below the two tricritical points it is of first order. There is a rather strong asymmetry present in the phase diagram; however, to a large extent

this is simply due to our normalization of the chemical potential, coming from the choice $\pi R^2/V_0 = \pi \neq 1$ (see discussion at the end of Sec. II). Indeed, when choosing the more natural normalization $V_0 = \pi R^2$, i. e. plotting the phase diagram in the (μ_{eff}, T) -plane, the asymmetry is much weaker, but still present, as seen in Fig. 2. Since there are infinitely many possible normalizations for μ , all resulting in different phase diagrams with differing degree of asymmetry, we do not consider it useful to discuss the phase diagram's symmetry in the grand-canonical ensemble. This should rather be done in the (Θ, T) -plane, where the phase diagram is free of such trivial ambiguities.

In Fig. 3 we show this phase diagram, and compare it to the data obtained in Ref. [9] for (i) the same model as ours, but the elastic interactions turned off, and (ii) the same model as (i) in the Ising language, but a (ferromagnetic) three-body interaction added (for more details, see Ref. [9]). Clearly, the pure lattice-gas model with only pair interactions has a symmetric phase diagram. The inclusion of the three-body term induces a very strong asymmetry, such that the second tricritical point at higher coverages vanishes (or was undetectable within the resolution of Ref. [9]). Nevertheless, the shape of the second-order line $c(2 \times 2) \leftrightarrow$ disordered at high temperatures is remarkably insensitive to the three-body term (for further discussion, see also Ref. [13]). Conversely, the phase diagram of our model, which shows the effect of elastic interactions, is rather close to that of the “unperturbed” model in the whole plane. The highest critical temperature is reduced by a few percent, and the tricritical points' temperatures also seem to be somewhat reduced (note that we did not attempt to locate the tricritical points very accurately; the phase transitions at $T = 2.5$ still seem to be of second order). Altogether, we find a surprisingly small influence of the translational degrees of freedom. In fact, the asymmetry in our model's phase diagram is so weak that it can hardly be detected at all by just looking at Fig. 3. Therefore, Fig. 4 compares the data for $0 \leq \Theta \leq 1/2$ with the mirror image of the phase diagram in the range $1/2 \leq \Theta \leq 1$, with symbols larger than the error bars.

B. Details of Calculation

At low temperatures, where the phase transitions are of first order, we studied an $L = 100$ system for 10^4 MCS per state point. This system size was large enough to make hysteresis well observable in sweeps of μ back and forth through the transition. For example, Fig. 5 studies the transition $(1 \times 1)_- \leftrightarrow c(2 \times 2)$ at $T = 2$, where a clear hysteresis is visible in the staggered magnetization. The transition occurs somewhere within the loop, and the corresponding ranges are indicated in Fig. 1 and Fig. 2. A more accurate determination of the transition chemical potential μ_{tr} would require thermodynamic integration procedures. For example, one could use the method outlined in Ref. [26], or the Frenkel-Ladd procedure [31]. This was however not attempted, since it turned out that a reasonably accurate determination of the (Θ, T) phase diagram was possible without accurate knowledge of μ_{tr} , simply because the hysteresis loops of Θ (data not shown) are all rather flat.

For the second-order phase transitions at higher temperatures we used finite-size scaling (FSS) [32,33] procedures. We chose linear paths in the (μ, T) -plane (not necessarily parallel to the axes) and studied the fourth-order cumulant U_L along them for the system sizes $L = 10, 20, 30$. For example, Fig. 6 shows the data for a rather high temperature. One sees that the intersection point, which serves as estimate for the critical point, is quite well defined. Therefore the method allowed a rather accurate determination of the second-order transition line. The intersection properties deteriorate somewhat when approaching the

tricritical points, which we did not attempt to localize very accurately. We also tried W_L intersection plots; however, we found that this method would not provide more accurate estimates from our data than the analysis of U_L .

C. Critical Behavior

The cumulant intersection value in Fig. 6 is around 0.62, a value which is typically obtained in simulations of the two-dimensional Ising universality class [34]. Of course, this is just the universality class which is expected for a one-dimensional order parameter as ours [5,6]. However, the translational degrees of freedom gave us a reason to nevertheless check the critical behavior: In related three-dimensional models of binary alloys [26,27] Mean-Field like critical behavior had been found, due to an effective long-range interaction mediated by the elastic distortions. In the present model, however, Mean Field behavior can be clearly ruled out, since in this case one expects [26,32,35] a cumulant value of roughly 0.3. This is further corroborated by the data collapsing plots for the staggered magnetization shown in Fig. 7 (Ising) and Fig. 8 (Mean Field). There we check the standard FSS relations [32] ($t = T/T_c - 1$ denoting the normalized distance to the critical point)

$$\langle |m_{st}| \rangle = L^{-\beta/\nu} \tilde{m}_{st} \left(L^{1/\nu} t \right), \quad (4.1)$$

for Ising universality ($\beta = 1/8$, $\nu = 1$), and

$$\langle |m_{st}| \rangle = N^{-1/4} \tilde{m}_{st} \left(N^{1/2} t \right), \quad (4.2)$$

for the Mean Field case, where $N = L^2$ is the total number of sites. Note that in this special case the arguments of the scaling functions coincide, while the prefactors differ strongly. A comparison of Fig. 7 with Fig. 8 clearly shows that our data are better described by Ising-like behavior than Mean Field. A similar conclusion can be drawn from susceptibility data (not shown), where the relation

$$\chi_{st} = L^{\gamma/\nu} \tilde{\chi}_{st} \left(L^{1/\nu} t \right) \quad (4.3)$$

for Ising-like behavior with $\gamma = 1.75$ is checked against the Mean Field relation

$$\chi_{st} = N^{1/2} \tilde{\chi}_{st} \left(N^{1/2} t \right). \quad (4.4)$$

For the present model the translational degrees of freedom obviously have no influence on the universality class.

V. SUMMARY AND DISCUSSION

The present work proposes a new modeling approach for Monte Carlo simulation studies of adsorbed monolayers. The elastic lattice gas is a hybrid between a lattice model and a continuum model, allowing us to include the translational degrees of freedom of the latter, while retaining the tight data structure of the former, which permits an algorithm which is conceptually simple and computationally efficient. The presented treatment shows how to deal with the statistical mechanics of the vacancies or “ghost particles” in a consistent and efficient way; the introduction of the confining square-well potential U_0 is a crucial

feature. Nevertheless, starting from the derived effective Hamiltonian, one could try to improve the efficiency even further. For example, by decoupling the pseudospin flips from the translational motion, one could use force-biased MC [29] for the latter, and perhaps also develop a cluster flip method [36] for the former. Both the theoretical treatment as well as the simulation data show that the inclusion of the elastic degrees of freedom destroys the inherent particle-hole symmetry present in simple lattice gases with pair interactions. Moreover, the theoretical analysis shows that the chemical potential at nonzero temperatures is only defined up to an additive constant, which is fixed by prescribing a value for the partition function normalization volume V_0 . Therefore, one should view the phase diagram in the grand-canonical ensemble only as an auxiliary diagram with no direct physical meaning. As far as the phase diagram in the canonical ensemble is concerned, we observed a surprisingly small influence of the elastic degrees of freedom, both with respect to the induced asymmetry, as well as with respect to the location of the phase boundaries. This is even more astonishing when one considers the fact that the elastic lattice was chosen as very soft (probably even beyond what is physically reasonable), such that large fluctuations in the positions of the adatoms occur. These fluctuations also have no influence on the critical behavior; the two-dimensional Ising universality class remains unchanged. While we expect that this latter result should also be true for more realistic elastic lattice gases, it is not clear how strongly the phase diagram's insensitivity to the elastic degrees of freedom depends on the additional simplifying features which we introduced, i. e. mainly the restriction to harmonic potentials, and the disregard of any mismatch between the adsorbate-adsorbate and the adsorbate-substrate interaction. It is certainly worthwhile to study these questions further by systematically lifting these restrictions, and introducing more realistic models.

ACKNOWLEDGMENTS

We thank the computer center at the University of Kaiserslautern (RHRK) for generous allocation of Cray time. This research was supported in part by NSF grant No. DMR-9405354, and NATO grant No. CRG 921202.

REFERENCES

- [1] *Ordering in two Dimensions*, edited by S. K. Sinha (North-Holland, Amsterdam, 1981).
- [2] P. Piercy and H. Pfnür, Phys. Rev. Lett. **59**, 1124 (1987).
- [3] D. H. Baek and J. W. Chung, Phys. Rev. B **47**, 8461 (1993).
- [4] C. Voges, K. Budde, and H. Pfnür, Surf. Sci. **338**, L839 (1995).
- [5] M. Schick, Progr. Surf. Sci. **11**, 245 (1981).
- [6] E. Domany, M. Schick, J. S. Walker, and R. B. Griffiths, Phys. Rev. B **18**, 2209 (1978).
- [7] K. Binder and D. P. Landau, Adv. Chem. Phys. **76**, 91 (1989).
- [8] D. P. Landau, Phase Transitions in Surface Films **2**, 11 (1990).
- [9] K. Binder and D. P. Landau, Surf. Sci. **108**, 503 (1981).
- [10] K. Binder, W. Kinzel, and D. P. Landau, Surf. Sci. **117**, 232 (1982).
- [11] A. Milchev and K. Binder, Surf. Sci. **164**, 1 (1985).
- [12] B. Dünweg, A. Milchev, and P. A. Rikvold, J. Chem. Phys. **94**, 3958 (1991).
- [13] T. L. Einstein, Langmuir **7**, 2520 (1991).
- [14] P. Piercy, K. De'Bell, and H. Pfnür, Phys. Rev. B **45**, 1869 (1992).
- [15] B. N. J. Persson, Surf. Sci. **258**, 451 (1991).
- [16] S. W. Koch and F. F. Abraham, Phys. Rev. B **33**, 5884 (1986).
- [17] N.-T. Vu, A. Jakalian, and D. B. Jack, J. Chem. Phys. **106**, 2551 (1997).
- [18] K. Binder, in *Monte Carlo Methods in Statistical Physics*, edited by K. Binder (Springer-Verlag, Berlin, 1986).
- [19] J. P. Valleau and L. K. Cohen, J. Chem. Phys. **72**, 5935 (1980).
- [20] L. A. Rowley, D. Nicholson, and N. G. Parsonage, J. Comp. Phys. **17**, 401 (1975).
- [21] N. Georgiev, A. Milchev, M. Paunov, and B. Dünweg, Surf. Sci. **264**, 455 (erratum 275, 493) (1992).
- [22] N. B. Wilding and A. D. Bruce, J. Phys.: Condens. Matter **4**, 3087 (1992).
- [23] N. B. Wilding, Phys. Rev. E **52**, 602 (1995).
- [24] W. W. Wood, in *Physics of Simple Liquids*, edited by H. N. V. Temperley, J. S. Rowlinson, and G. S. Rushbrooke (North-Holland, Amsterdam, 1968).
- [25] A. Z. Panagiotopoulos, in *Observation, Prediction and Simulation of Phase Transitions in Complex Fluids*, edited by M. Baus, L. F. Rull, and J.-P. Ryckaert (Kluwer Academic Publishers, Dordrecht, 1995).
- [26] B. Dünweg and D. P. Landau, Phys. Rev. B **48**, 14182 (1993).
- [27] M. Laradji, D. P. Landau, and B. Dünweg, Phys. Rev. B **51**, 4894 (1995).
- [28] M. Nielsen *et al.*, Phys. Rev. E **54**, 6889 (1996).
- [29] M. P. Allen and D. J. Tildesley, *Computer Simulation of Liquids* (Clarendon, Oxford, 1987).
- [30] K. Binder, Z. Phys. **B 43**, 119 (1981).
- [31] D. Frenkel and A. J. C. Ladd, J. Chem. Phys. **81**, 3188 (1984).
- [32] B. Dünweg, in *Monte Carlo and Molecular Dynamics of Condensed Matter Systems*, edited by K. Binder and G. Ciccotti (Societa Italiana di Fisica, Bologna, 1996).
- [33] *Finite Size Scaling and Numerical Simulation of Statistical Systems*, edited by V. Privman (World Scientific, Singapore, 1990).
- [34] D. P. Landau and D. Stauffer, J. de Physique **50**, 509 (1989).
- [35] E. Brezin and J. Zinn-Justin, Nucl. Physics **B 257**, 867 (1985).
- [36] J. E. Gubernatis and N. Kawashima, in *Monte Carlo and Molecular Dynamics of Condensed Matter Systems*, edited by K. Binder and G. Ciccotti (Societa Italiana di Fisica, Bologna, 1996).

FIGURES

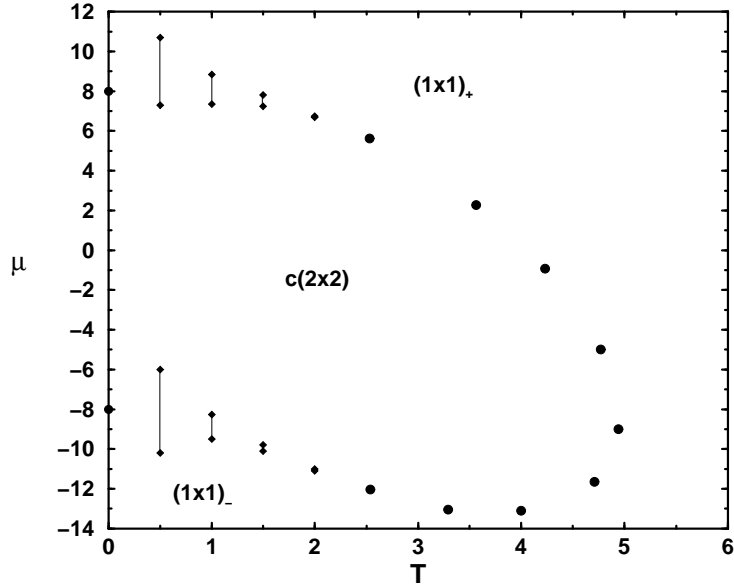


FIG. 1. The phase diagram of the elastic model specified in Eqn. 2.2, and at the beginning of Sec. III, in the grand-canonical ensemble ((μ, T) -plane). Second-order phase transitions at high temperatures are indicated by filled circles. The error in the location of these transitions is smaller than the symbol size. The intervals bracketed by diamonds indicate the possible range for the location of first-order transitions at lower temperatures.

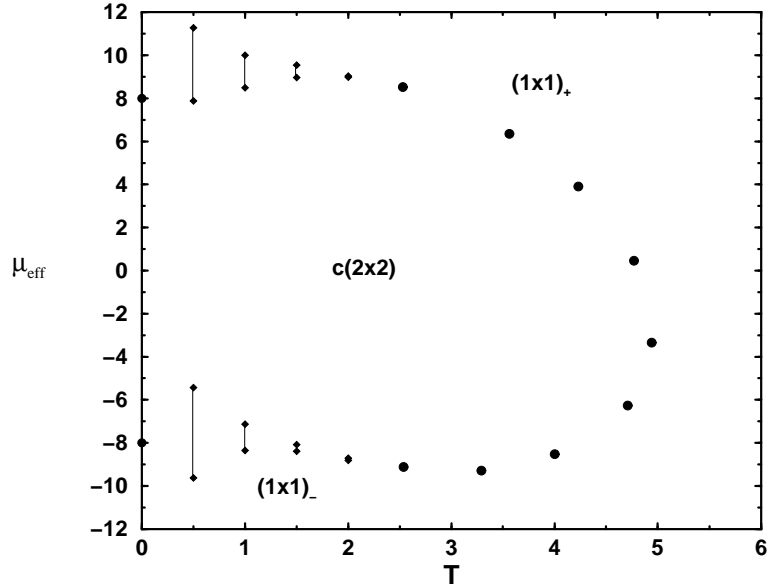


FIG. 2. Same as Fig. 1, but using a different normalization for the chemical potential, such that instead of μ there appears the effective chemical potential $\mu_{\text{eff}} = \mu + k_B T \ln \zeta$ (see text).

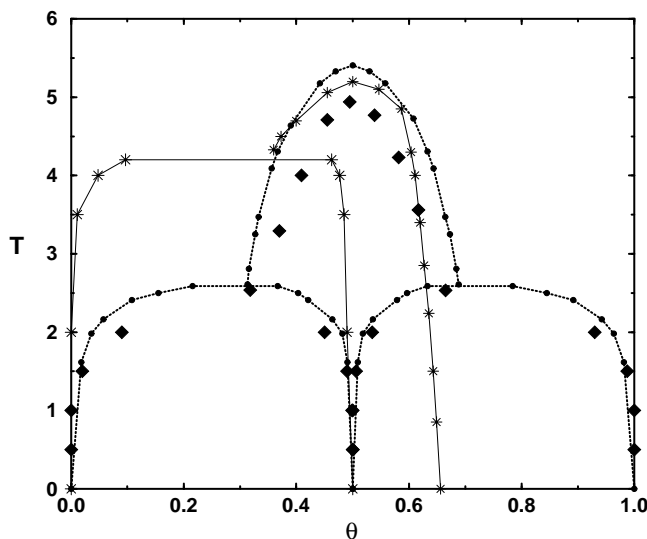


FIG. 3. The phase diagram in the canonical ensemble ((Θ, T) -plane). (i) Filled circles: Lattice-gas / Ising model with antiferromagnetic nearest-neighbor interaction, and ferromagnetic next-nearest neighbor interaction (Ref. [9]). (ii) Asterisks: Same Ising model as (i), but a ferromagnetic three-body interaction added (Ref. [9]). (iii) Filled diamonds: Model of the present study, which would reduce to (i) if the elastic interactions were turned off. The second-order phase transition line at high temperatures ends in tricritical points below which two-phase regions open up: $c(2 \times 2)$ and $(1 \times 1)_+$ at high coverages; $c(2 \times 2)$ and $(1 \times 1)_-$ at low coverages. In case (ii), the two-phase region at high coverages is not present.

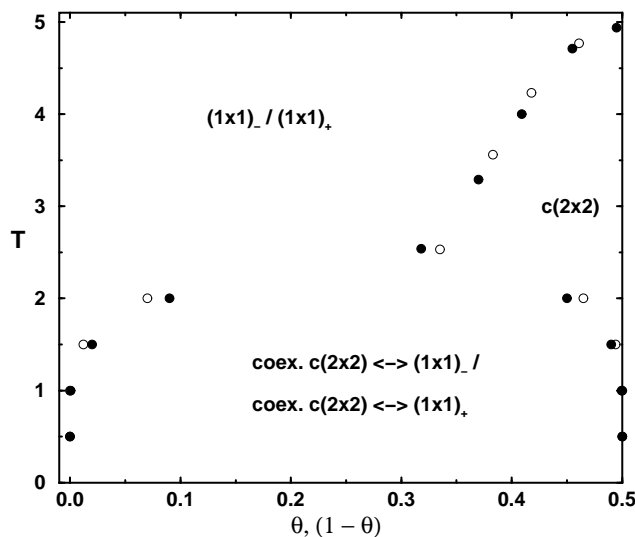


FIG. 4. The phase diagram of the elastic model specified in Eqn. 2.2, and at the beginning of Sec. III, in the canonical ensemble ((Θ, T) -plane). In order to demonstrate the weak asymmetry, we have superimposed the data for Θ in the range $0 \leq \Theta \leq 1/2$ (filled circles) with those for $1 - \Theta$ in the range $1/2 \leq \Theta \leq 1$ (open circles). Error bars are always smaller than the symbol sizes.

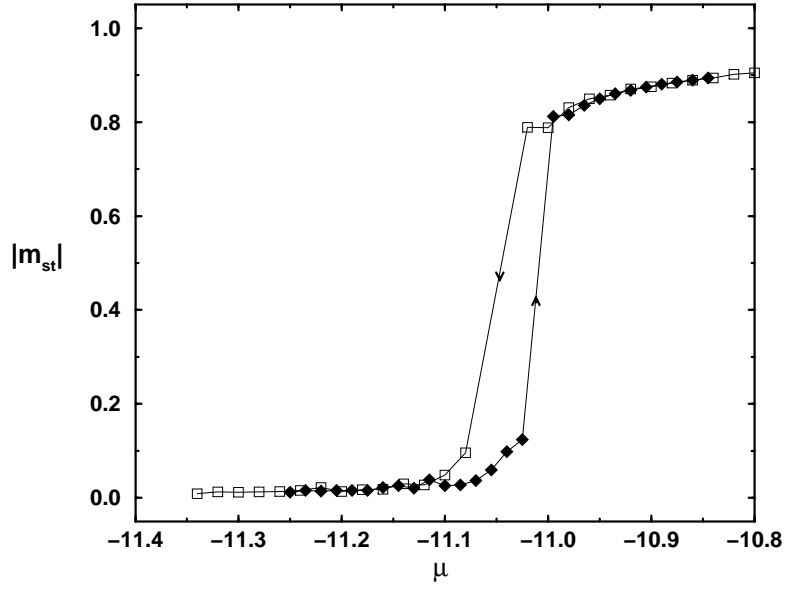


FIG. 5. Hysteresis loop of $|m_{st}|$ as a function of μ , for $T = 2$.

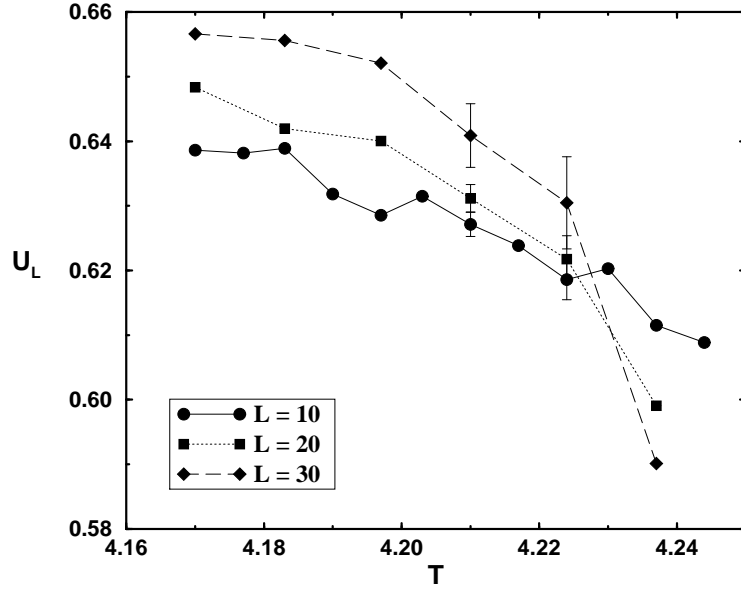


FIG. 6. Cumulant intersection plot for U_L , and three system sizes. Both T and μ were varied along a linear path in the (μ, T) -plane in the range $(\mu, T) = (-1.25, 4.17)$ and $(\mu, T) = (-0.8375, 4.2437)$. Characteristic error bars are shown.

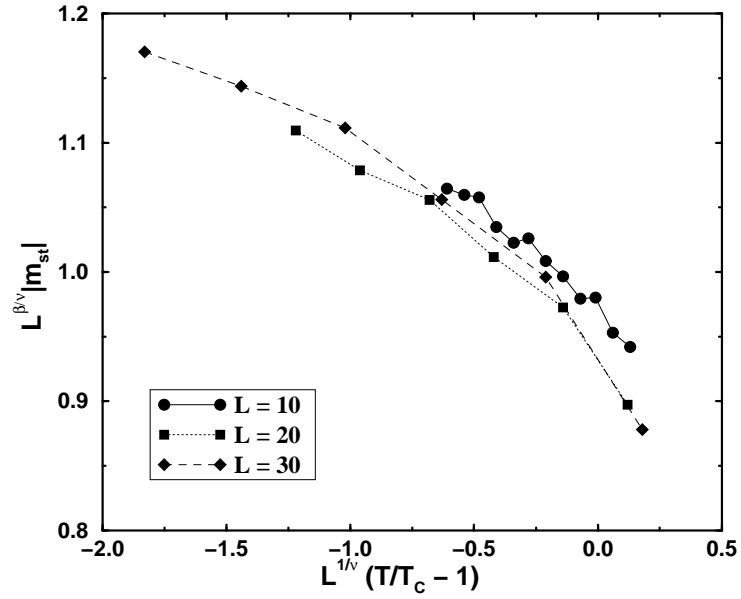


FIG. 7. Finite-size scaling plot for order parameter data near the second-order transition at $\mu = \mu_c = -0.930$, $T = T_c = 4.231$, using the critical exponents of the two-dimensional Ising universality class, $\beta = 1/8$, $\nu = 1$. For Ising-like critical behavior, the data for the different system sizes $L = 10, 20, 30$ should all lie on a single curve. Data are for the same path in the phase diagram as those of Fig. 6.

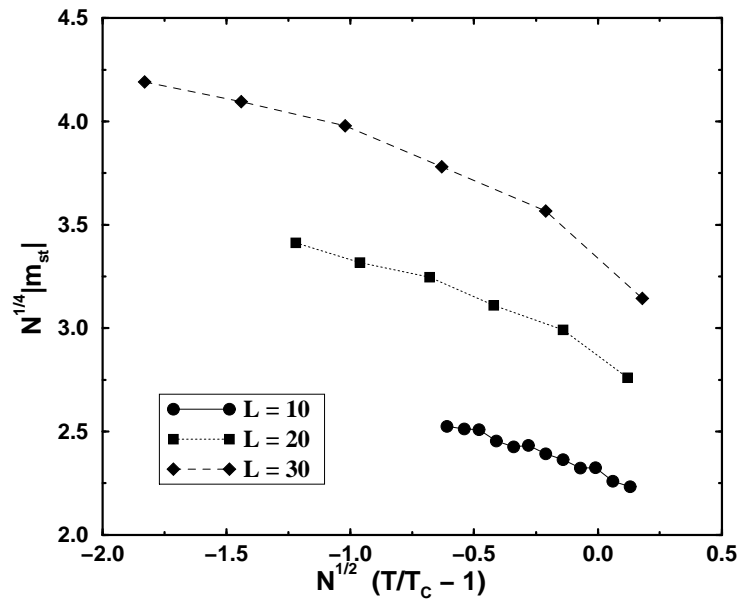


FIG. 8. Same as Fig. 7, but plotted using Mean-Field like critical exponents.